

Contact Information Flow and Design of Compliance

Kevin Haninger, Marcel Radke, Richard Hartisch, Jörg Krüger

Abstract

Identifying changes in contact during contact-rich manipulation can detect task state or errors, enabling improved robustness and autonomy. The ability to detect contact is affected by the mechatronic design of the robot, especially its physical compliance. Established methods can design physical compliance for many aspects of contact performance (e.g. peak contact force, motion/force control bandwidth), but are based on time-invariant dynamic models. A change in contact mode is a discrete change in coupled robot-environment dynamics, not easily considered in existing design methods.

Towards designing robots which can robustly detect changes in contact mode online, this paper investigates how mechatronic design can improve contact estimation, with a focus on the impact of the location and degree of compliance. A design metric of information gain is proposed which measures how much position/force measurements reduce uncertainty in the contact mode estimate. This information gain is developed for fully- and partially-observed systems, as partial observability can arise from joint flexibility in the robot or environmental inertia. Hardware experiments with various compliant setups validate that information gain predicts the speed and certainty with which contact is detected in (i) monitoring of contact-rich assembly and (ii) collision detection.

1 Introduction

Manipulation aims to achieve a relative arrangement of objects, often with a desired set of contacts between them. In structured environments, this desired contact can be achieved with a certain robot pose, but as robots are applied in less-structured environments, the required robot pose may vary. A robot which can robustly detect contact mode can improve autonomy, for example using online contact detection to switch the controller [1] or to provide a reward signal to a learning process [2].

We call a *contact mode* a constraint over generalized robot and environment position q , i.e. $\phi_i(q) = 0$ for the i^{th} mode. This is often considered an infinitely stiff kinematic constraint in robotics, either eliminated or enforced with impulses in time-stepping approaches [3]. Here, we consider a compliant contact model where forces are measured over position

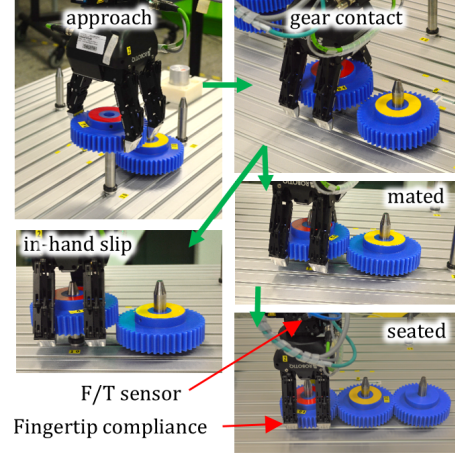


Figure 1: Contact-rich manipulation task, where a discrete collection of contact dynamics occur, corresponding to different task phases. Detecting these changes can help error monitoring like in-hand slip, and the ability to detect these changes is a function of sensor placement and physical dynamics.

q [4, 5]. Contact can also be described with an inequality $\phi_i(q) \geq 0$ to describe non-penetration of rigid bodies [3, 6], but we separate the contact conditions into discrete contact modes with equality constraints [5].

Contact mode can be used for task representation and planning. As the contact depends on surface geometry, contact modelling is more common in locomotion where flat surfaces simplify the expression of $\phi(q)$ [6]. In manipulation, when constraints are simple and known in advance, a task can be represented as a sequence of contact modes [7], which can then be used for motion planning [8, 9]. Contact geometry can also be demonstrated with special instruments [10]. Data-based methods have been used, learning contact geometry on simplified geometries [11], but not yet demonstrated on robotic manipulation.

Offline contact models are not robust to variation in environmental objects [12], which can be improved with on-line detection of contact. Estimation of environment dynamics has been established, using a Kalman filter to estimate environment stiffness [13] or impedance [5]. In locomotion, foot contact mode estimation has been proposed in a stochastic framework [1], shown to improve robustness to unexpected changes in floor height. In manipulation, discrete contact mode estimation has been proposed through recursive Bayesian estimation [14–16] and support vector ma-

Authors affiliated with the Department of Automation at Fraunhofer IPK, Berlin, Germany. Corresponding email: kevin.haninger@ipk.fraunhofer.de. This project has received funding from the European Union’s Horizon 2020 research and innovation programme under grant agreement No 820689 – SHERLOCK.

chines [17].

The ability to sense contact mode is affected by the hardware design. Hardware design also affects peak collision force [18–20], and contact stability [21, 22]. The location, degree and structure of compliance can be designed to improve energy efficiency [23, 24], reduce the need for information [25], or reduce the problem dimension [26]. Compliance can have negative effects, reducing the feasible feedback control gain [27] and the effectiveness of feedforward control [28], limiting motion control performance.

The contribution of this paper is a method to design compliance to improve estimation of the contact mode. The estimation of contact mode is established [1, 14–16], but the impact of mechatronic design on this estimation is not yet investigated. Analytical rules for ‘distinguishability’ of contact modes have been proposed [29], but the approach here considers compliance and sensor noise. This paper first introduces the compliant contact models, then the information gain from position and force measurements in the fully- and partially-observed case. The information gain is written in closed form for a linear inertial system. Finally, experiments validate that information gain predicts the certainty and speed of assembly monitoring and collision detection, where the location and degree of compliance is varied.

Notation

Random variables are typeset in boldface $\mathbf{n} \sim p(n)$. The normal distribution is denoted $\mathcal{N}(\mu, \Sigma)$, and $\mathcal{N}(x|\mu, \Sigma)$ denotes an evaluation of the Gaussian probability distribution function at x . Proportionality \propto indicates a distribution is written without a normalization constant for compactness. The matrix determinant \det , and can be ignored when the argument is scalar. A sequence of variables is denoted $q_{1:t} = [q_1, \dots, q_t]$.

2 Contact and robot models

This section presents the dynamic model for compliant contact and observation models for position and force.

2.1 Compliant robot model

Let the robot and environment be described by generalized position $q \in Q = \mathbb{R}^D$ with velocity \dot{q} . Compliance (in the joint, gripper, or environment) can then be modelled by adding to the standard manipulator equations of motion as [30]

$$M(q)\ddot{q} + \tau(q, \dot{q}) - K(q) = B(q)\tau_m, \quad (1)$$

where $M(q) \in \mathbb{R}^{D \times D}$ is the inertia matrix, $\tau(q, \dot{q}) \in \mathbb{R}^D$ contains the gravitational, Coriolis, and friction forces, spring-like forces $K : \mathbb{R}^D \rightarrow \mathbb{R}^D$, and input matrix $B(q) \in \mathbb{R}^{D \times K}$ modifies motor torque input $\tau_m \in \mathbb{R}^K$.

This model will be reduced to a two-mass model in the direction of contact motion, but provides the general statement for contact state and observations.

2.2 Contact State

Contact is modelled as an equality constraint over total configuration, $\phi(q) = 0$ [3]. A compliant contact model is used here [4, 5] instead of impulse-based [3] – it is assumed that sufficient compliance is present that collision forces can be represented as a function over configuration q .

While inequality constraints $\phi(q) \geq 0$ can capture non-penetration constraints, thereby modelling both free-space and constrained dynamics in a unified way [6], the approach here instead uses a collection of equality constraints, only one of which is active at once. Therefore, the contact state is then a discrete variable $n \in [1, \dots, N]$, where each contact state n has a corresponding constraint $\phi_n(q) = 0$.

2.3 Observation model

Denote a position measurement at time step t which measures some of the robot/environment positions $\theta_t \in \Theta \subset Q$, representing, e.g. that motor positions are measured, but the position of links or environmental inertias are not.

Let the measured torques/forces $f_t \in \mathbb{R}^L$ be a subset of the forces on compliant elements,

$$\mathbf{f}_t = K_f^n(q_t) + \epsilon_t \quad (2)$$

where $\epsilon_t \sim \mathcal{N}(0, \Sigma_f)$ is i.i.d. noise capturing electrical or quantisation noise, and $K_f^n : Q \rightarrow \mathbb{R}^L$ the effective sensor stiffness for the mode n . Therefore

$$p(f_t|n, q_t) = \mathcal{N}(K_f^n(q_t), \Sigma_f). \quad (3)$$

As force/torque sensors measure displacement – either strain or bulk displacement [31] – practical force measurements can be described with (2).

3 Contact Information Gain

Bayesian inference is used to recursively infer contact mode given a prior belief of contact mode, position and force measurements. The prior distribution can reflect a priori assumptions about the environment, e.g., that a contact occurs at a certain location, or it could be a belief informed by other sensors.

3.1 Fully Observed

When the system is fully observed, i.e. $\Theta = Q$, a prior belief $p(n)$ is updated by a measurement f , θ as

$$p(n|f, \theta) = \frac{p(f|n, \theta)p(n)}{\sum_{m=1}^N p(f|m, \theta)p(m)}, \quad (4)$$

where the denominator is a normalization constant.

In the fully observed case, multiple measurements are independent as ϵ_t in (2) is i.i.d., and the full posterior is

$$p(n|f_{1:t}, \theta_{1:t}) \propto p(n) \prod_{i=1}^t p(f_i|n, \theta_i). \quad (5)$$

This can be updated recursively as a hidden Markov model [32].

3.2 Partially observed

In the partially observed case, some positions are not directly measured. This can arise from joint flexibility (motor position is measured, link position is not), or from inertia in the environment. In this case, there are force contributions from the unmeasured inertias which will appear with the forces resulting from the contact mode.

We denote measured position θ_t and unmeasured position \bar{q}_t , so $q_t = [\theta_t^T, \bar{q}_t^T]^T$, making the force observation model $p(f_t | \bar{q}_t, \theta_t, n)$. A dynamic model such as a discretized version of (1) can be used for inference, where we assume the dynamics $p(\bar{q}_{t+1} | n, \bar{q}_t, \theta_t)$ are known (these are derived for linear inertial system in Section 4.2). With these dynamics, a standard recursive estimate can be written [32, Ch. 2.4]

$$p(\bar{q}_t | n, \theta_{1:t-1}, f_{1:t-1}) \propto \int p(\bar{q}_1) \prod_{i=1}^{t-1} p(\bar{q}_{i+1} | n, \bar{q}_i, \theta_i) p(f_i | n, \bar{q}_i, \theta_i) \bar{q}_{1:t-1}, \quad (6)$$

where $p(\bar{q}_1)$ is a distribution of initial position \bar{q}_1 . To calculate (6), a Kalman filter can be used in the linear case [32, Ch. 3.2], and in the nonlinear flexible-joint robot case, various observers of link-side position/velocity are established [33].

The observation model (3) then needs to be marginalized over \bar{q}_t as

$$p(f_t | n, f_{1:t-1}, \theta_{1:t}) = \int p(f_t | n, \bar{q}_t, \theta_t) p(\bar{q}_t | f_{1:t-1}, \theta_{1:t-1}, n) d\bar{q}_t. \quad (7)$$

We assume the force observations (2) are linear, i.e. $K_f^n(q_t) = K_f^n(q_t - q_0^n)$ where $K_f^n \in \mathbb{R}^{L \times D}$ and q_0^n is the rest position of the spring. Denote the posterior belief of $p(q_t | n, f_{1:t-1}, \theta_{1:t-1}) = \mathcal{N}(\mu_q^n, \Sigma_q^n)$, then the force measurement is distributed as

$$p(f_t | n, f_{1:t-1}, \theta_{1:t-1}) = \mathcal{N}(K_f^n(\mu_q^n - q_0^n), K_f^n \Sigma_q^n K_f^{n,T} + \Sigma_f). \quad (8)$$

Note that the covariance in \mathbf{f}_t now depends on the uncertainty in the position Σ_q^n , the stiffness K_f^n , and force sensor noise Σ_f .

3.3 Information gain

The information gain is proposed as the reduction in uncertainty from $p(n)$ to $p(n | f, \theta)$, i.e. how much a measurement reduces belief entropy. Recall that entropy measures the uncertainty of a discrete random variable $H(\mathbf{n}) = -\sum_{n=1}^N p(n) \ln(p(n))$ and differential entropy over continuous random variables $h(\mathbf{x}) = -\int p(x) \ln p(x) dx$ [34, Ch. 2], we define the information gain as

$$\Delta_I = H(\mathbf{n}) - H(\mathbf{n} | \mathbf{f}, \theta). \quad (9)$$

A larger Δ_I means that the measurement brings more certainty.

Denoting a belief vector $b \in \mathbb{R}^N$, where $p(n = m) = b_m$, $b_m > 0$, $\|b\|_1 = 1$, and the distribution of \mathbf{f} per mode as

$$p(f | n, \theta) = \mathcal{N}(f | \mu_n, \Sigma_n), \quad (10)$$

the following relations hold:

$$H(\mathbf{n} | \mathbf{f}, \theta) = H(\mathbf{n}) - h(\mathbf{f} | \theta) + h(\mathbf{f} | \mathbf{n}, \theta), \quad (11)$$

$$h(\mathbf{f} | \mathbf{n}, \theta) = \frac{L}{2} \ln 2\pi e + \sum_{n=1}^N \frac{b_n}{2} \ln \det \Sigma_n, \quad (12)$$

$$h(\mathbf{f} | \theta) \geq - \sum_{n=1}^N b_n \ln \left(\sum_{m=1}^N b_m \mathcal{N}(\mu_m | \mu_n, \Sigma_n + \Sigma_m) \right), \quad (13)$$

where (11) results from writing $I(\mathbf{f}, \mathbf{n} | \theta)$ two ways, $h(\mathbf{f} | \theta) - h(\mathbf{f} | \mathbf{n}, \theta) = H(\mathbf{n} | \theta) - H(\mathbf{n} | \mathbf{f}, \theta)$ [35], (12) is standard multivariate Gaussian entropy with the expectation taken over \mathbf{n} [34], and (13) is directly Theorem 2 of [36]. Then, Δ_I can be lower bounded as $\Delta_I \geq \underline{\Delta}_I$ where

$$\underline{\Delta}_I = - \sum_{n=1}^N b_n \ln \sum_{m=1}^N b_m \mathcal{N}(\mu_n | \mu_m, \Sigma_n + \Sigma_m) - \frac{L}{2} \ln 2\pi e - \sum_{n=1}^N \frac{b_n}{2} \ln \det \Sigma_n. \quad (14)$$

To demonstrate, the information gain bound $\underline{\Delta}_I$ with two modes $N = 2$, one dimension $L = 1$, and a flat prior belief $b_n = 0.5$ is shown in Figure 2, where $\mu_1 = 0$, $\Sigma_1 = 1$, and μ_2, Σ_2 are varied. The minimum is reached when $\mu_2 = 0$, $\Sigma_2 = 1$, where the two distributions are identical. As Σ_2 decreases, the information gain increases, as well as when $|\mu_2 - \mu_1|$ increases. Note that the information gain saturates - the maximum reduction in uncertainty is the prior uncertainty $H(\mathbf{n})$.

Interpreting this for the contact mode, when the mean force expected from two contacts vary widely, a force measurement should provide more information gain and the mode uncertainty should decrease quickly. If the mean of the force expected in the two modes is the same, there may be some information gain as long as the covariance is different. However, if the mean and covariance of two contact mode forces are the same, there is no reduction in mode uncertainty.

In the partially-observed case, $\underline{\Delta}_I = H(\mathbf{n}) - H(\mathbf{n} | \mathbf{f}_t, f_{1:t-1}, \theta_{1:t})$, modifying the force distribution (10).

4 Information gain in inertial systems

In this section, information gain is considered on a linear, inertial system as seen in Figure 3. We consider that force is measured as $f_t = K_1(q_t^2 - q_t^1) + \epsilon_t$, where $\epsilon_t \sim \mathcal{N}(0, \Sigma_f)$.

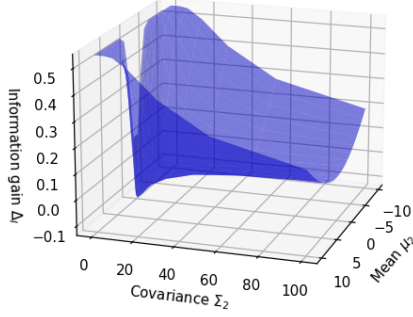


Figure 2: Information gain for single observation with two modes, where $\mu_1 = 0$, $\Sigma_1 = 1$. As the differences between the two distributions increase, the information gain increases, and the mode can be more accurately inferred.

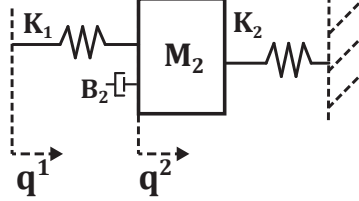


Figure 3: Linear inertial model, where q^1 is measured robot or motor position, and q^2 possibly unmeasured.

Consider two modes, free space where $K_1 = 0$, and contact with M_2 where $K_1 > 0$. This gives

$$\begin{aligned} p(f|n=1) &= \mathcal{N}(0, \Sigma_f) \\ p(f|n=2, q^1, q^2) &= \mathcal{N}(K_1(q^1 - q^2), \Sigma_f). \end{aligned} \quad (15)$$

4.1 Fully observed

In the fully observed case, the positions of q^1, q^2 are known and there are no unmeasured inertias. In other words, the robot is stiff, the environment has no inertias, and the contact force model (3) can be directly evaluated. If we consider the information gain at a flat prior $b_n = 0.5$, (14) can be used with (15) to find

$$\begin{aligned} \Delta_I(q^1, q^2) &= -\ln(\mathcal{N}(0|K_1(q^1 - q^2), 2\Sigma_f)) \\ &\quad - \frac{1}{2} \ln 2\pi e - \frac{1}{2} \ln \Sigma_f \\ &= \frac{1}{2} K_1^2 (q^1 - q^2)^2 (2\Sigma_f)^{-1} - \frac{1}{2} (1 - \ln 2), \end{aligned} \quad (16)$$

using $\mathcal{N}(\mu_n|\mu_m, \Sigma_n + \Sigma_m) = \mathcal{N}(\mu_m|\mu_n, \Sigma_n + \Sigma_m)$.

Here, we note that the information gain increases as K_1 does, $|q^1 - q^2|$ grows, or as sensor noise Σ_f decreases. When we have a stiff environment, deeper contact, or a less noisy sensor, the ability to estimate contact mode increases.

4.2 Partially observed

Here we consider when q^2 is not observed, e.g. q^1 is motor position and q^2 is the position of an environment or link inertia. The contact force model (3) cannot be directly evaluated, first q^2 must be estimated, increasing uncertainty. As time is relevant in the partially observed case, we denote q_t^1 and q_t^2 as the values at time step t , and consider that q_t^1 is measured, along with force as in (15). The first-order discretized system dynamics can be written as

$$\begin{aligned} \begin{bmatrix} q_{t+1}^2 \\ \dot{q}_{t+1}^2 \end{bmatrix} &\approx \begin{bmatrix} 1 & T_s \\ -T_s \frac{K_2 + K_1}{M_2} & 1 - T_s \frac{B_2}{M_2} \end{bmatrix} \begin{bmatrix} q_t^2 \\ \dot{q}_t^2 \end{bmatrix} \\ &\quad + \begin{bmatrix} 0 \\ T_s M_2^{-1} K_1 \end{bmatrix} q_t^1 + \begin{bmatrix} 0 \\ M_2^{-1} \end{bmatrix} \mathbf{w}_t \\ &= A \begin{bmatrix} q_{t+1}^2 \\ \dot{q}_{t+1}^2 \end{bmatrix} + B q_t^1 + B_w \mathbf{w}_t \end{aligned} \quad (18)$$

where $\mathbf{w}_t \sim \mathcal{N}(0, \Sigma_w)$ is i.i.d. process noise which is assumed to be a force disturbance, and thus multiplied by M_2^{-1} .

A Kalman estimator can be written, where, for simplicity, we consider the covariance of $p(q_t^2|f_{1:t}, q_{1:t}^1)$ as $t \rightarrow \infty$, which is given by the steady-state covariance of P , which satisfies the discrete algebraic Riccati equation of

$$P = A P A^T - A P C^T (C P C^T + \Sigma_f)^{-1} C P A^T + B_w \Sigma_w B_w^T, \quad (19)$$

where A, B and B_w are from (18) and $C = [K_1, 0]$ [32].

While the steady-state covariance P is not necessarily the covariance during transient phases (i.e. when starting from an uncertain initial condition), it has a simple closed-form solution which is differentiable [37].

With this assumption, $p(q_t^2|f_{1:t-1}, q_{1:t-1}^1) \sim \mathcal{N}(\mu_t^2, P^+)$, where $P^+ = A P A^T + B_w \Sigma_w B_w^T$ and the posterior distribution on \mathbf{f}_t can be written as:

$$\begin{aligned} p(f_t|n=2, q_{1:t}^1, f_{1:t-1}) &= \\ &\mathcal{N}(K_1(\mu_t^2 - q_t^1), K_1 P^+ K_1^T + \Sigma_f), \end{aligned} \quad (20)$$

updating the contact force distribution in (15).

5 Experimental Results

We test information gain in experiments with industrial robots (7 and 60 Kg payload) and varying compliant conditions. An F/T sensor is integrated at the flange and measured at 1250 Hz, and a standard admittance control and collision detector implemented, see [38] for details. When collision is detected based on a force threshold, the position commanded to the robot is held to the last position before collision was detected. The F/T sensors used in all setups have similar noise properties, and $\Sigma_f = 1.25$ is used for all conditions.

The experimental data and analysis code is available at <https://owncloud.fraunhofer.de/index.php/s/ovt0lGRb7o7b9Fb>.

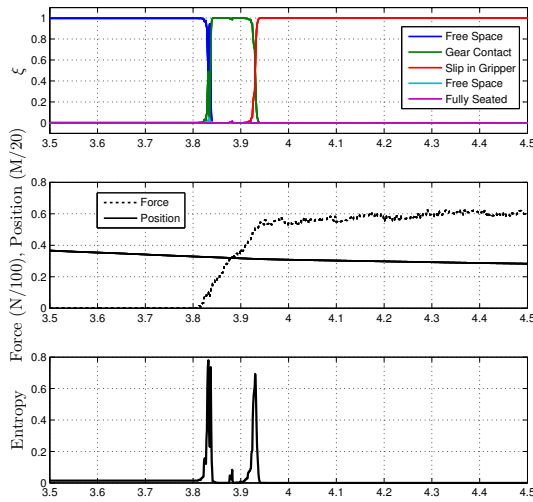


Figure 4: Detail of transition in mode estimate, with estimated contact state over time (top), force/position (middle) and belief entropy at each time step (bottom).

5.1 Monitoring Assembly

We consider an admittance-controlled gear assembly task from [16], where the gear assembly has multiple stages, as seen in Figure 1. One failure mode is in-hand slip, which may occur during the gear mating process. We modify the setup by introducing additional foam at the fingertips, between the gripper and gear, and compare the ability to infer the task mode. The parameters of the estimator are available with the experimental data in the above mentioned cloud folder.

A typical mode detection from a trial with in-hand slip can be seen in Figure 4, where the belief entropy (i.e. mode uncertainty) increases substantially during the transitions between the modes. Comparing the total entropy over a number of experiment iterations, we find that decreasing the gripper stiffness increases the total uncertainty, as seen in Figure 5.

The information gain is calculated using the fully-observed information gain (17) with the gripper stiffness as K_1 , and the average taken over $|q^1 - q^2| \in [0, 0.5]$ mm with a flat prior $b_n = 1/N$. It can be seen that the higher stiffness has higher information gain, corresponding with lower total belief entropy.

5.2 Collision detection - High Payload Robot

A 16 Kg plate is mounted to a large industrial robot as seen in Figure 7, and brought into contact with a compliant magazine, where compliance is introduced in one of three locations: (i) in the joints of the magazine, (ii) on the contact surface, and (iii) under the feet of the magazine. The robot was driven into contact in using admittance control with a desired contact force of 30 N. Pure admittance control is used to collect data for model identification, then contact detection is activated, where a simple force threshold of 6 N is used (gravitational forces of the plate are compensated).

As seen in Figure 6, the fastest contact detection occurred with compliance on the feet (bottom), where the hard contact

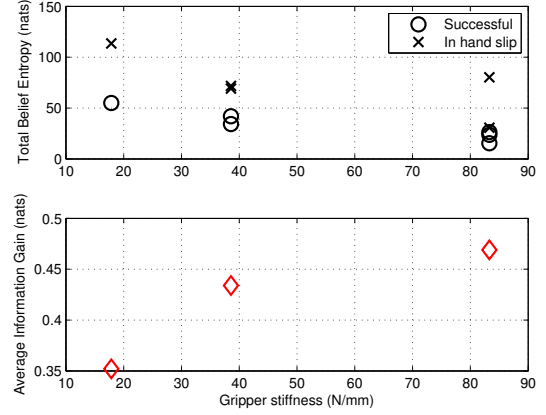


Figure 5: Total belief entropy over compliance at the gripper. For both successful and in hand slip trials, the uncertainty increases as the compliance decreases.

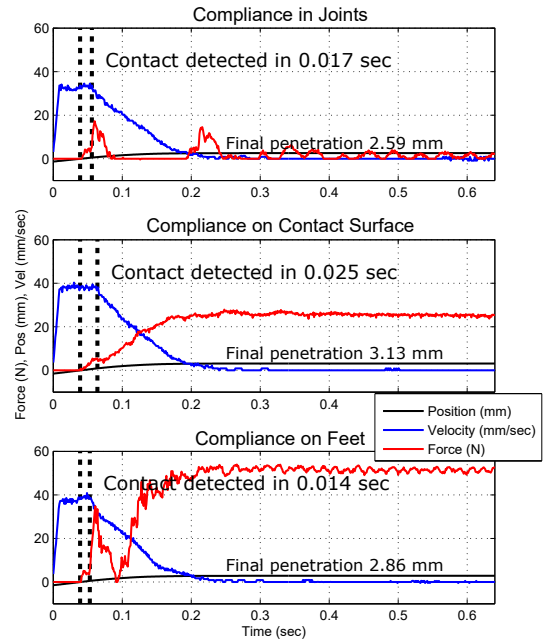


Figure 6: Contact force, position, and velocity in experiments with the contact detection

Condition	K_1	M_2	B_2	K_2	$\underline{\Delta}_I$
Flex Joints	17.4e4	20.1	305	2630	0.131
Compliant Surface	1.3e4	63.9	1870	7350	0.0743
Compliant Feet	2.61e4	69.3	1080	1.81e4	0.348
Flex Joints Gradient	7.7e-6	7.6e-3	2.2e-6	-4.8e-10	-
Comp Surf Gradient	1.5e-5	1.8e-3	1.7e-6	1.3e-10	-
Comp Feet Gradient	2.5e-5	0.8e-3	1.3e-6	4.8e-10	-

Table 1: Identified dynamic parameters for the magazine contact

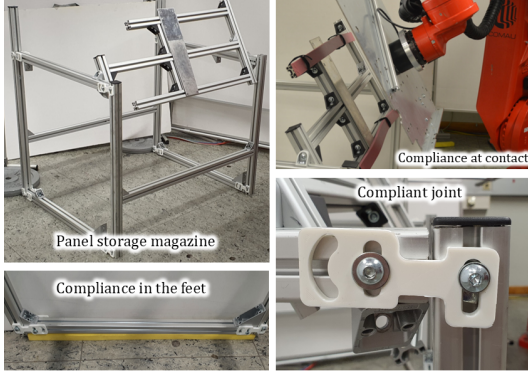


Figure 7: Contact magazine with the various locations of compliance, using strips of viscoelastic foam, or 3d printed flexure joints.

and larger effective magazine inertia results in an initial peak in force. Compliance in the joints results in the 2nd fastest contact detection – note that in this case contact was lost as the magazine springs back with the lower K_2 . The slowest contact detection was with compliance at the contact surface, where force increases slowly.

A model for these three compliance cases is then identified following the inertial model in Figure 3, where the measured robot position is q^1 , unmeasured magazine position is q^2 and the measured force is that on K_1 . These parameters are identified by doing a least-squares fit $\min_{K_1, M_2, B_2, K_2} \sum_t \|f_t^m - f_t^m\|$, where f_t^m is the model output given the observed q_t^1 as input, and can be seen in Table 1, with time plots in Figure 8.

From these models, the $\underline{\Delta}_I$ can be calculated in the partially observed case with q_t at time $t = 0.002$. It can be seen in Table 1 that the compliant feet has the highest information gain, followed by the compliant joints and compliant surface, corresponding to the contact detection performance. Because the $\underline{\Delta}_I$ calculation is composed of differentiable operations, the gradient can be numerically calculated with an automatic differentiation toolbox [39], also seen in Table 1. It can be seen that increasing K_1 and M_2 make the largest increase in $\underline{\Delta}_I$, while B_2 and K_2 play a more minor role. The gradient validates an experimental observation: a higher contact inertia M_2 helps improve contact detection.

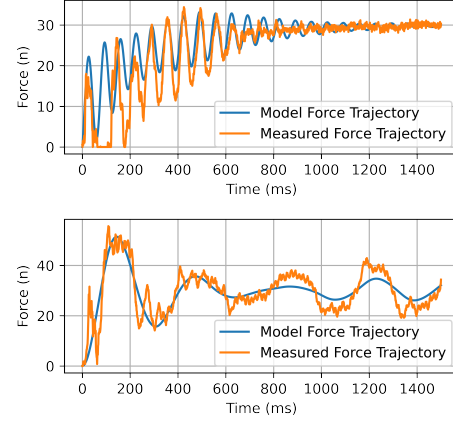


Figure 8: Identified model and real response, for flex joint magazine (top) and compliance in the feet (bottom). Contact is made with force control, with desired force of 30 N. Note that admittance parameters are set poorly for the bottom contact, but the identified model is still accurate.

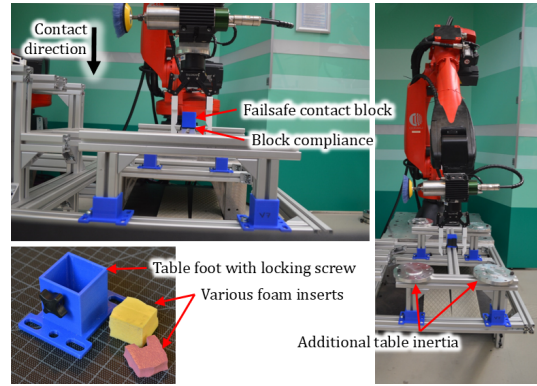


Figure 9: Compliant table with 7 Kg payload robot, where compliance can be adjusted in the feet of the table or between the failsafe block and table.

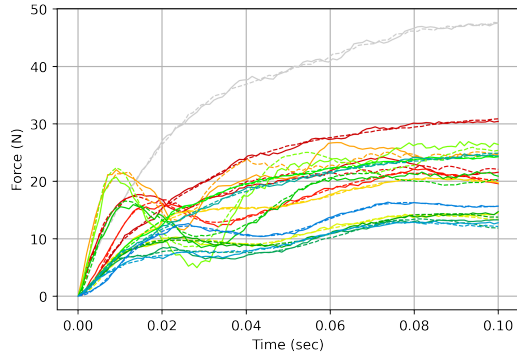


Figure 10: Traces of contact force (solid line) vs identified model response (dotted). Detailed responses can be better seen on the online repository, these responses show the range of force profiles and model fit.

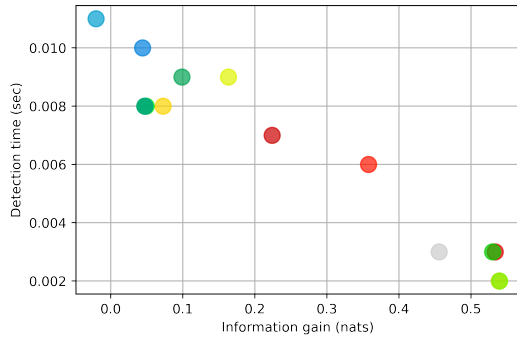


Figure 11: Information gain vs time to detect contact, colors are consistent with those used in Figure 10. As information gain increases, the time required to detect contact decreases. Hard contact and higher table inertia gave the fastest detection.

5.3 Collision Detection - Medium Payload Robot

A compliant table, seen in Figure 9, was used to investigate the impact of location and quantity of compliance on the ability to detect contact. By varying the compliance in the feet and contact surface, as well as the inertia of the table, a range of contact responses were achieved as seen in Figure 10. A simple contact detection threshold of 6 N was applied, and the performance can be seen in the attached video. Model identification was done as above, but a two-inertia model was found to provide better model fit, requiring a straightforward extension to (18) which is omitted due to space constraints but in the published code.

The information gain, calculated with (20) at the state $t = 0.002$ after contact, is compared with the time taken to detect the contact in Figure 11. It can be seen that as information gain increases, time to detect contact decreases.

The configurations where contact compliance was removed, and where additional weight was added to the table, had higher information gain and a higher contact velocity could be safely achieved - further detailed plots are available online with the experimental data.

6 Conclusion

The impact of mechatronic design, especially compliance, on the ability to detect contact conditions was presented, and formalized in a metric of the information gain. This metric is validated to predict the certainty with a complex assembly task can be monitored, and the speed with which collision can be detected.

In the case of introducing compliance to the environment, it is shown that this compliance is best introduced not at the point of contact, but deeper into the kinematic structure. This allowed faster contact detection in both the magazine and table contact tasks.

References

- [1] G. Bledt, P. M. Wensing, S. Ingersoll, and S. Kim, "Contact Model Fusion for Event-Based Locomotion in Unstructured Terrains," in *2018 IEEE International Conference on Robotics and Automation (ICRA)*, May 2018, pp. 4399–4406.
- [2] M. Vecerik, O. Sushkov, D. Barker, T. Rothörl, T. Hester, and J. Scholz, "A Practical Approach to Insertion with Variable Socket Position Using Deep Reinforcement Learning," *arXiv:1810.01531 [cs]*, Oct. 2018.
- [3] D. E. Stewart, "Rigid-Body Dynamics with Friction and Impact," *SIAM Review*, vol. 42, no. 1, pp. 3–39, Jan. 2000.
- [4] A. M. Castro, A. Qu, N. Kuppaswamy, A. Alspach, and M. Sherman, "A Transition-Aware Method for the Simulation of Compliant Contact With Regularized Friction," *IEEE Robotics and Automation Letters*, vol. 5, no. 2, pp. 1859–1866, Apr. 2020.
- [5] M. V. Minniti, R. Grandia, K. Fähr, F. Farshidian, and M. Hutter, "Model predictive robot-environment interaction control for mobile manipulation tasks," in *2021 IEEE International Conference on Robotics and Automation (ICRA)*. IEEE, 2021, pp. 1651–1657.
- [6] M. Posa, C. Cantu, and R. Tedrake, "A direct method for trajectory optimization of rigid bodies through contact," *The International Journal of Robotics Research*, vol. 33, no. 1, pp. 69–81, 2014.
- [7] Feng Pan and J. M. Schimmels, "Robust procedures for obtaining assembly contact state extremal configurations," in *IEEE International Conference on Robotics and Automation, 2004. Proceedings. ICRA '04. 2004*, vol. 1, Apr. 2004, pp. 972–977 Vol.1.
- [8] J. De Schutter, T. De Laet, J. Rutgeerts, W. Decré, R. Smits, E. Aertbeliën, K. Claes, and H. Bruyninckx, "Constraint-based task specification and estimation for sensor-based robot systems in the presence of geometric uncertainty," *The International Journal of Robotics Research*, vol. 26, no. 5, pp. 433–455, 2007.

- [9] M. P. Polverini, A. M. Zanchettin, and P. Rocco, "A constraint-based programming approach for robotic assembly skills implementation," *Robotics and Computer-Integrated Manufacturing*, vol. 59, pp. 69–81, 2019.
- [10] W. Meeussen, J. Rutgeerts, K. Gadeyne, H. Bruyninckx, and J. De Schutter, "Contact-state segmentation using particle filters for programming by human demonstration in compliant-motion tasks," *IEEE Transactions on Robotics*, vol. 23, no. 2, pp. 218–231, 2007.
- [11] S. Pfrommer, M. Halm, and M. Posa, "Contact-Nets: Learning of Discontinuous Contact Dynamics with Smooth, Implicit Representations," *arXiv preprint arXiv:2009.11193*, 2020.
- [12] J. Rosell, L. Basanez, and R. Suárez, "Contact Identification for robotic assembly tasks with uncertainty," *IFAC Proceedings Volumes*, vol. 33, no. 27, pp. 141–146, 2000.
- [13] L. Roveda, "Sensorless environment stiffness and interaction force estimation for impedance control tuning in robotized interaction tasks," *Autonomous Robots*, p. 18.
- [14] I. F. Jasim and P. W. Plapper, "Contact-state recognition of compliant motion robots using expectation maximization-based Gaussian mixtures," in *ISR/Robotik 2014; 41st International Symposium on Robotics; Proceedings Of*. VDE, 2014, pp. 1–8.
- [15] T. Ren, Y. Dong, D. Wu, and K. Chen, "Collision detection and identification for robot manipulators based on extended state observer," *Control Engineering Practice*, vol. 79, pp. 144–153, 2018.
- [16] K. Haninger and D. Surdilovic, "Multimodal Environment Dynamics for Interactive Robots: Towards Fault Detection and Task Representation," in *Proc. IEEE/RSJ Intl Conf on Intelligent Robots and Systems (IROS)*, 2018, pp. 6932–6937.
- [17] S. Golz, C. Osendorfer, and S. Haddadin, "Using tactile sensation for learning contact knowledge: Discriminate collision from physical interaction," in *2015 IEEE International Conference on Robotics and Automation (ICRA)*. IEEE, 2015, pp. 3788–3794.
- [18] P. M. Wensing, A. Wang, S. Seok, D. Otten, J. Lang, and S. Kim, "Proprioceptive Actuator Design in the MIT Cheetah: Impact Mitigation and High-Bandwidth Physical Interaction for Dynamic Legged Robots," *IEEE Transactions on Robotics*, vol. 33, no. 3, pp. 509–522, Jun. 2017.
- [19] A. Bicchi and G. Tonietti, "Fast and "Soft-Arm" Tactics," *IEEE Robotics & Automation Magazine*, vol. 11, no. 2, pp. 22–33, Jun. 2004.
- [20] K. Haninger and D. Surdilovic, "Bounded Collision Force by the Sobolev Norm: Compliance and Control for Interactive Robots," in *2019 IEEE International Conference on Robotics and Automation (ICRA)*, 2019, pp. 8259–8535.
- [21] S. D. Eppinger and W. P. Seering, "Three dynamic problems in robot force control," *IEEE Transactions on Robotics and Automation*, vol. 8, no. 6, pp. 751–758, 1992.
- [22] G. Pratt and M. Williamson, "Series elastic actuators," in *1995 IEEE/RSJ International Conference on Intelligent Robots and Systems 95. 'Human Robot Interaction and Co-operative Robots', Proceedings*, vol. 1, Aug. 1995, pp. 399–406 vol.1.
- [23] E. A. Bolivar-Nieto, G. C. Thomas, E. Rouse, and R. D. Gregg, "Convex Optimization for Spring Design in Series Elastic Actuators: From Theory to Practice," 2021.
- [24] S. Haddadin, K. Krieger, A. Albu-Schäffer, and T. Lilge, "Exploiting elastic energy storage for "blind" cyclic manipulation: Modeling, stability analysis, control, and experiments for dribbling," *IEEE Transactions on Robotics*, vol. 34, no. 1, pp. 91–112, 2018.
- [25] K. Haninger, "Minimum directed information: A design principle for compliant robots," in *IEEE International Conference on Robotics and Automation (ICRA)*, 2021.
- [26] M. Hamaya, R. Lee, K. Tanaka, F. von Drigalski, C. Nakashima, Y. Shibata, and Y. Ijiri, "Learning robotic assembly tasks with lower dimensional systems by leveraging physical softness and environmental constraints," in *2020 IEEE International Conference on Robotics and Automation (ICRA)*. IEEE, 2020, pp. 7747–7753.
- [27] P. Tomei, "A simple PD controller for robots with elastic joints," *Automatic Control, IEEE Transactions on*, vol. 36, no. 10, pp. 1208–1213, 1991.
- [28] C. Della Santina, M. Bianchi, G. Grioli, F. Angelini, M. Catalano, M. Garabini, and A. Bicchi, "Controlling Soft Robots: Balancing Feedback and Feedforward Elements," *IEEE Robotics Automation Magazine*, vol. 24, no. 3, pp. 75–83, Sep. 2017.
- [29] T. J. Debus, P. E. Dupont, and R. D. Howe, "Distinguishability and identifiability testing of contact state models," *Advanced Robotics*, vol. 19, no. 5, pp. 545–566, 2005.
- [30] M. W. Spong, "Modeling and control of elastic joint robots," *Journal of dynamic systems, measurement, and control*, vol. 109, no. 4, pp. 310–318, 1987.
- [31] N. Kashiri, J. Malzahn, and N. G. Tsagarakis, "On the Sensor Design of Torque Controlled Actuators: A Comparison Study of Strain Gauge and Encoder-Based Principles," *IEEE Robotics and Automation Letters*, vol. 2, no. 2, pp. 1186–1194, Apr. 2017.
- [32] S. Thrun, "Probabilistic robotics," *Communications of the ACM*, vol. 45, no. 3, pp. 52–57, 2002.
- [33] S. Haddadin, A. De Luca, and A. Albu-Schäffer, "Robot collisions: A survey on detection, isolation, and identification," *IEEE Transactions on Robotics*, vol. 33, no. 6, pp. 1292–1312, 2017.

- [34] T. M. Cover, *Elements of Information Theory*. John Wiley & Sons, 1999.
- [35] A. Kolchinsky and B. D. Tracey, “Estimating mixture entropy with pairwise distances,” *Entropy*, vol. 19, no. 7, p. 361, 2017.
- [36] M. F. Huber, T. Bailey, H. Durrant-Whyte, and U. D. Hanebeck, “On entropy approximation for Gaussian mixture random vectors,” in *2008 IEEE International Conference on Multisensor Fusion and Integration for Intelligent Systems*. IEEE, 2008, pp. 181–188.
- [37] T.-C. Kao and G. Hennequin, “Automatic differentiation of Sylvester, Lyapunov, and algebraic Riccati equations,” *arXiv:2011.11430 [cs, math]*, Nov. 2020.
- [38] K. Haninger, M. Radke, A. Vick, and J. Kruger, “Towards High-Payload Admittance Control for Manual Guidance with Environmental Contact,” *IEEE Robotics and Automation Letters*, 2022.
- [39] J. A. Andersson, J. Gillis, G. Horn, J. B. Rawlings, and M. Diehl, “CasADi: A software framework for nonlinear optimization and optimal control,” *Mathematical Programming Computation*, vol. 11, no. 1, pp. 1–36, 2019.